TÉCNICO LISBOA

# MEMS resonators in dissipative media - Towards the detection of biomolecules

Guilherme Ricardo Mendes da Silva Barreto de Figueiredo

*Abstract* - **MEMS resonators can operate as mass sensors for biological applications due to their label free, small size and low power consumption properties. The principle is based on the addition of analyte molecules that bind to the surface of the structures, inducing a resonance frequency shift. MEMS should be measurable at atmospheric pressure and liquid media to enable the detection of biomolecules. For this work several hydrogenated amorphous silicon microbridges were fabricated on glass substrates at temperatures below 200 ºC. The structures were electrostatically actuated and optically measured at ~$10^{-2}$ Torr, with resonance frequencies in the range of MHz and quality factors (Q-factors) of ~1000, for structures between 40 µm and 200 µm in length. To assess if MEMS devices are suitable for biological detection, several dissipation mechanisms were tested. To verify the hypothesis that molecules at the surface of the structures can affect the Q-factors, *annealing* temperatures up to 250 ºC were applied. It was demonstrated that the Q-factors improved on all of the samples. The structures were also measured at atmospheric pressure and immersed in DI water. These media considerably affects the operability of the structures, which is confirmed by the large decrease of the Q-factors, where the highest value in liquid medium is 17.**

## I. Introduction

MICROELECTROMECHANICAL systems (MEMS) contain micro scale structures that can be fabricated with several components ranging from 1 to 100 µm (micrometers) in size. As the name implies, these systems are composed by an electric component in a form of an external power supply used for both actuation and detection. The term mechanical comes from its ability to perform vertical or lateral mechanical motions or actions, depending on the type of structure, and how it is being actuated.

The growing need to develop new point-of-care portable devices that can detect specific biomolecules in liquid media, led to an increase in the investigations of MEMS, focused on medical and public health applications.

In order to maintain the majority of their functionalities, many biological reactions and biomolecules need aqueous environments so, it is imperative to have quantitative, real-time and *in situ* measurements for biosensing [1].

Liquid-phase measurements are a complex challenge due to the damping effects of liquid environments, which causes considerable quality factor (Q-factor) reduction [2]. This reduction can be quite extensive, depending on the properties of the structures, and can range from 1000-10000 down to 1-10, also accompanied by a loss of sensitivity. One of the goals of this work is to bypass this reduction since the minimal detectable mass for these types of sensors will be dependent on the Q-factor of the structures.

To use MEMS devices for biodetection, one should increase its detection sensitivity, which can be achieved by playing with several parameters and characteristics of the structures including the optimization of the damping effects that can be done by operating the devices at higher order vibrational modes, the selection of specific materials that induce higher Q-factors, the reduction of the structures thickness during the microfabrication process, and also the selection of a more suitable geometry for both the structure itself and the actuating gates [2] [3].

In this work, several measurements in different media such as vacuum, air and DI water were performed, along with pressure experiments to detect the critical pressures at which Q-factor values begin to decrease. *Annealing* experiments were also performed with temperatures up to 250 ºC in an attempt to increase the intrinsic Q-factors of the structures.

## II. Microfabrication Process

During this work, several runs were developed to fabricate the desired MEMS structures to be characterized, along with older devices previously fabricated.

Since the fabrication process of the majority of the devices is similar, it will be described here the last microfabrication sequence performed.

Since the substrate used for the development of the devices mentioned above is glass, two Corning 1737 glass slides of 50x25 mm and 0,7 mm of thickness were selected, cleaned in an Alconox solution for 30 minutes to 1 hour, depending on the dust and dirt particles initially present on the substrate, and placed in a bath with ultrasounds and a temperature of about 65 ºC. After this process, the slides were washed with deionized (DI) water and then blow dried using a compressed air gun.

After the preparation of the substrates, they are suitable to enter the clean room environment to start the microfabrication process. One layer of titanium tungsten (TiW) with 100 nm of thickness was deposited using a Nordiko 7000 machine. The next step was the first lithography. After a pre-treatment that consisted on a coating with a photoresist, a mask previously designed in AutoCad, where the first layer mask, corresponding to the gates was used to pattern the TiW, in the DWL machine. In this specific case a positive photoresist was used, meaning that the area that is exposed to the laser becomes soluble to the developer that is used to remove the excess photoresist, at the end of the process.

The following process was performed in LAM machine, and was a reactive ion etch (RIE) which was used to remove the excess TiW around the gates. For these samples the process took around 450 seconds. It is important to start with shorter time frames and then perform a visual inspection to see if the excess TiW was removed, because too much etching time will start to etch the gates itself. After this etch the samples are immersed in a solution of Microstrip in order to remove the excess photoresist left from the lithography process. The samples are then removed, washed with acetone and $H_2O$, and dried with a compressed air gun. This run included structures with different lengths and also with different number of gates *per* structure (one, two and four).

Nordiko 7000 machine was used again in order to deposit 1 μm of Aluminum (Al) that served as the sacrificial layer , that is the layer that will be between the gates and the structures itself that later was removed leaving the structures suspended. The process is equal to the one mentioned above except that the target is different, so the particles deposited on the samples are from Al instead of TiW.

The second lithography was the next step. The pre-treatment was equal to the first one and the second layer mask corresponding to the sacrificial layer was used to pattern the samples. Since it was the second layer, it was fundamental to use the alignment marks present in each layer, to make sure that the consequent layer is perfectly aligned with the previous one. The consequent etching process was a wet etch where a chemical solution containing acids, bases or alcohols is used. For this case an Al etchant was used which is an acid solution to selectively remove Al. This procedure takes between 10 and 15 minutes. The samples were then submersed in $H_2O$ and dried with a compressed air gun. Then the excess photoresist from the lithography was removed using Microstrip, washed with acetone and $H_2O$ and dried again. The structural layer of the structures is made of a-Si:H which was deposited by RF-PECVD. For these samples, low stress was induced, by using an $H_2$ content of 73%. 1 μm of a-Si:H was deposited to create the structural layer, with a deposition time of 1 hour. In Nordiko 7000, 100 nm of TiW were then deposited on top of the a-Si:H, in order to create a metallic conductive surface on top of the structures. This also allowed skipping an additional lithography step to do the bridges and the pads separately, since the etching process could be done on both of the materials simultaneously. The last lithography step was made, in the same manner of the previous ones, including the coating, the alignment of the third layer mask, and the

development. Another RIE was then made in LAM on order to etch both a-Si:H and TiW. It was made in two runs, first during 300 seconds and a second one during 150 seconds, separated by a visual inspection to guarantee that there was no over etching. After this step, the samples were submersed in Microstrip to remove the excess photoresist, washed with acetone and $H_2O$, and dried. After this process is finished, the samples were covered with photoresist, which will function as a protective layer, so the structures will not be destroyed during the cutting of the individual dies.

Since the dies were all fabricated on the same samples, Disco DAD 321 machine was used to separate the dies from each other. This machine did 6.5 mm by 6.5 mm cuts for this case. To finish, the samples were exposed to UV light. Subsequently the dies were separated, and the last process to be done is the release of the structures, by removing the Al sacrificial layer present between the gates and the bridges. The photoresist used to protect the samples during the cutting was removed with Microstrip, washed with acetone and $H_2O$ and dried. This wet etching process involves four liquids with different surface tensions, and the samples were submersed sequentially from the higher surface tension to the lower. This is done so the structures do not collapse or get stuck to the substrate. The liquids are Al etchant, $H_2O$, Isopropyl alcohol (IPA) and n-hexane.

Figure 1 shows the final results after the complete microfabrication process. It is possible to observe that the sacrificial layer was removed, and the structures are suspended. In amplification, bridges of 50, 80 and 150 μm with one, two and four gates can be seen.

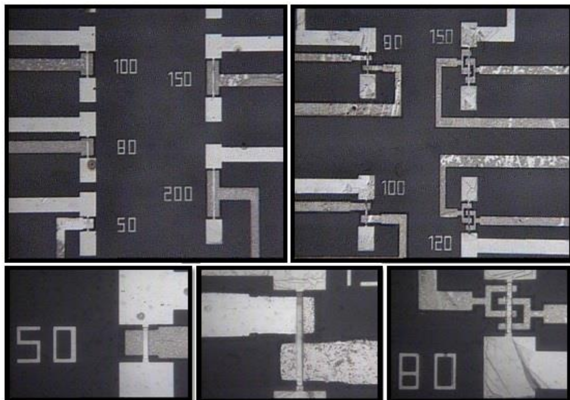


Figure 1 - Micrographs of several structures after their release

For this process as it was mentioned before, two glass substrates were used. For each of the substrates, two rows of six dies were fabricated, one row containing dies with single gate structures while the second row has structures with both two and four gates, in a total of twenty four devices, twelve with one gate, and twelve with two and four gates.

In order to get the devices ready to be optically characterized, the dies were glued onto chip carriers containing several pins that can be fitted in a special socket to allow for the passage of current into the structures.

To connect the chip carriers to the dies, one last step before any measurement can be done must be performed. That process is called wire bonding and consists on a special machine that is used to connect small thin aluminum wires from the chip carrier to the die, to allow the passage of current from an external source to the structures, which will induce the vibration of the structures. After this, the chips are ready to be used for any kind of measurements. The structures fabricated in this process range from 50 μm to 200 μm, depending on the design of the masks, and all of them have a width of 10 μm.

# III. Results and Discussion

## *A. Voltage Bias Sweep*

Due to the small size of MEMS devices, there is an inherent limitation on the stored energy and signal-to-noise ratio, which can impact the frequency stability of MEMS. In order to avoid this limitation of the output power it is possible to drive resonators into higher vibration amplitudes, which may cause the structures to operate in a nonlinear regime. The source of those nonlinearities can be classified as mechanical or electrical [4].

Graphic 1 shows a voltage bias measurement of the second vibrational mode of a bridge with 80 μm in length, 10 μm of width, 0.9 μm of thickness and a gap of 1 μm between the gate and the bridge. The sacrificial layer was Al.

For this situation, the effective stiffness of the structure is smaller at high amplitudes due to electrical softening, causing a specific response of the structure leading it to progressively bend towards the lower frequency side, as the applied DC voltage increases [5].

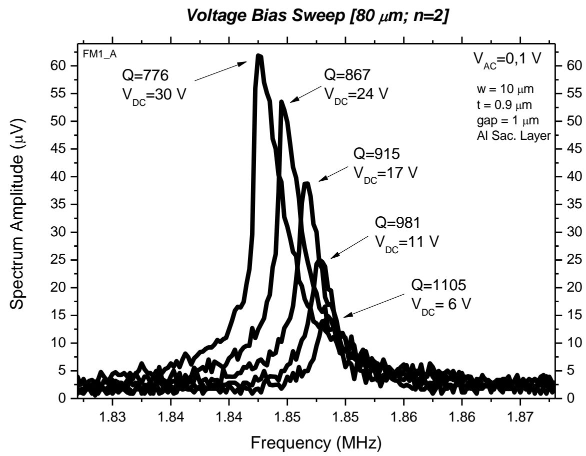


Graphic 1 - Voltage bias Sweep representation of a 80 µm bridge. E=150 GPa; ρ=2330 Kg/m$^3$; Pressure≈10$^{-2}$ Torr

Graphic 2 shows a voltage bias sweep measurement of the forth vibrational mode of a bridge with 120 µm in length, 10 µm of width, 0.9 µm of thickness and a gap of 1 µm between the gate and the bridge. The sacrificial layer was Al.

For this structure, the extracted peaks bend towards higher frequency values as the DC voltage increases, due to the mechanical stiffening of the effective spring constant at higher amplitudes.

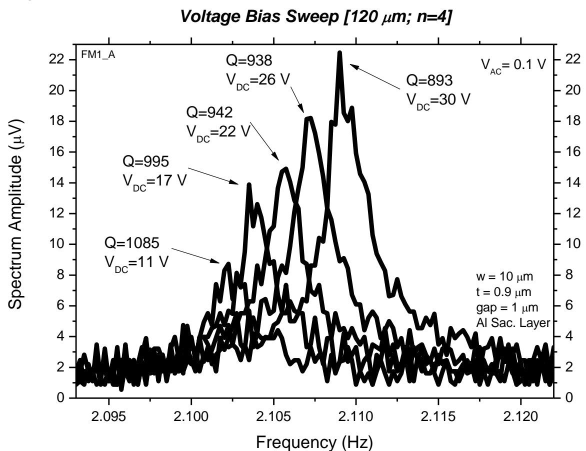


Graphic 2 - Voltage bias Sweep representation of a 120 µm bridge. E=150 GPa; ρ=2330 Kg/m$^3$; Pressure≈10$^{-2}$ Torr

Graphic 3 shows a voltage bias sweep measurement of the third vibrational mode of a bridge with 150 µm in length, 10 µm of width, 0.9 µm of thickness and a gap of 1 µm between the gate and the bridge. The sacrificial layer was Al.

An intermediate effect combining the electrical softening and the mechanical stiffening discussed above can also be visible as shown in Graphic 3.

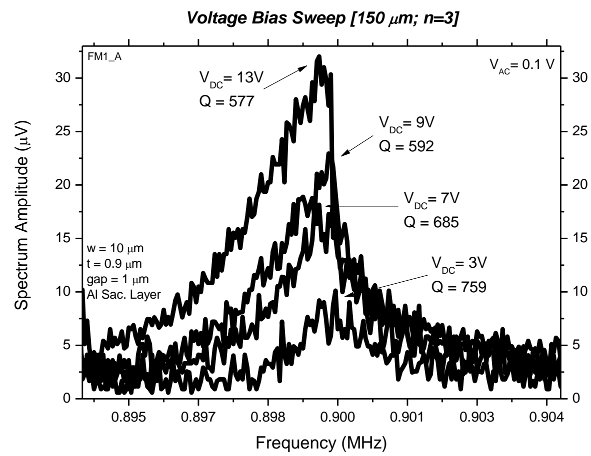


Graphic 3 - Voltage bias Sweep representation of a 150 µm bridge. E=150 GPa; ρ=2330 Kg/m$^3$; Pressure≈10$^{-2}$ Torr

For intermediate voltages a combination between mechanical and electrical effects can occur. For this particular structure, as amplitude increases, an electrical softening effect is visible to a certain point, followed by a mechanical stiffening effect, crossing a point at which their forces are balanced and cancel each other out. Due to this alteration of the mentioned effects, some amplitudes of oscillation are present where the frequency dependence for small amplitude perturbations can be neglected [5].

Also for this structure, the voltage applied was considerably lower, since the resonance peak started to create a nonlinear aspect at 9 V. That effect is much clearer at 13 V, where the right side of the peak is not symmetric to the left side.

To avoid the destruction of the structure, the voltage bias sweep was stopped at that voltage.

Despite Graphics 1, 2 and 3 represent only a few resonance peaks at certain voltages, these measurements were performed with a range of applied voltages starting from the minimal DC voltage possible to extract a resonance peak, with an increase of 1 V for each measurement, reaching 30 V or until a nonlinearity of the resonance peak became visible.

## *B. Annealing Measurements*

Several applications for MEMS resonators such as mass sensors, frequency references or accelerometers, can be quite sensitive to temperature induced frequency shifts that can induce errors into their output frequency. It is important to confirm that high Q-factors will be

available at elevated temperatures since it can be used as a direct measure of a resonators temperature if that Q-factor has strong dependence on temperature [6].

Some of the known energy loss mechanisms in microscale resonators are losses due to chemical impurities, surface quality, intentional or unintentional surface coating, hydration and surface losses, which can be improved or avoided after the fabrication manufacturing processes [6] [7].

The devices were exposed to a range of temperatures from 100 ºC to 250 ºC, with an increase of 25 ºC for each cycle of temperature exposure, during a period of 30 minutes *per* cycle, so these chips were exposed to 7 different *annealing* temperatures, 100 ºC, 125 ºC, 150 ºC, 175 ºC, 200 ºC, 225 ºC and 250 ºC. The room temperature was assumed to be 25 ºC and the maximum temperature of 250 ºC was selected after some measurements reaching 275 ºC showed that the structures were destroyed or the chips were badly burned.

Between each cycle, the devices were measured in vacuum, after a 10 minutes period of cooling at room temperature.

One of the chips after being subjected to the *annealing* temperatures was characterized for the fundamental mode regarding the *Fres* of its structures. It was observed that there were no major shifts in those frequencies. Despite those shifts were quite small, they appear to increase as the temperature rises for longer structures which may indicate that for much higher annealing temperatures and longer structures, that shift may also increase significantly. The Q-factor was also extracted for the fundamental mode of these structures and it is represented in Graphic 4.

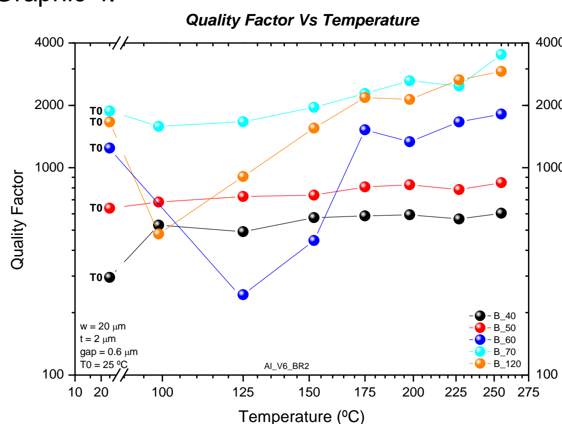

Graphic 4 - Quality Factor as a Function of the Annealing Temperature

After analyzing these preliminary annealing affected Q-factor results, it is clear that temperature significantly improves its value, thus reducing energy losses [7].

One could also reach a conclusion that, by looking at these results, there may be a certain threshold (for the results of Graphic 4, and merely speculative, Q=1000), were the Q-factors in the fundamental vibrational mode of the structures significantly decreases at lower annealing temperatures for initial Q-factors higher than 1000, and then significantly increases for higher annealing temperatures, as opposed to structures with lower initial Q-factors where there are slight increases in their values for lower annealing temperatures,  and the values for higher annealing temperatures are not that high when compared to what they initially were.

This hypothesis could also be considered for the length of the structures, where the shorter structures will be below this hypothetical threshold, while the longer structures will be above it.

Graphic 5 demonstrates in a more appealing manner this relation that the Q-factor has with the lower and higher annealing temperatures.

The 40 µm and 50 µm bridges present lower increases in their Q-factors while the longer structures tend to significantly improve them.

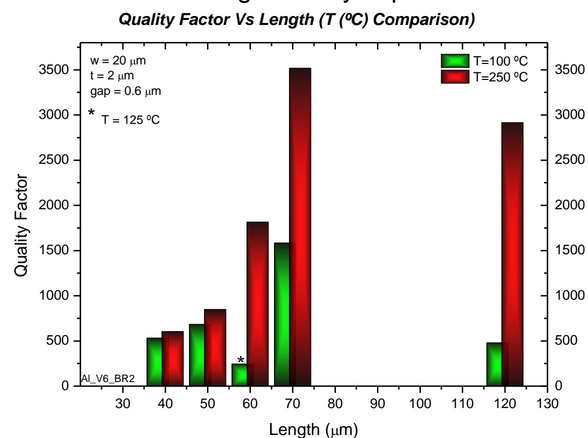

Graphic 5 - Annealing Temperature comparison of the Quality Factor as a function of Length

Another device from the same run with the same dimensions was also used for the annealing experiments in order to serve as a comparison with the previous device, and was also tested for different vibrational modes.

Despite the Q-factor of some of those structures demonstrated the same behavior of the previous device regarding an initial decrease at lower annealing temperatures followed by an

increase at higher temperatures, that behavior appears to be somewhat random thus compromising the idea of a threshold.

When analyzing the results from Graphic 4, it was discussed a possible threshold limit where the Q-factor of a given structure, typically a higher Q-factor, will decrease for lower annealing temperatures and increase significantly for higher ones. In that results, the threshold limit considered was Q=1000. By analyzing the results from the devices used for comparison, it was verified that their structures possessed Q-factor values at lower annealing temperatures higher than 3000, but a significant increase of those values was not present similar to the results from Graphic 4. This may indicate that, for higher modes, that threshold limit would be higher too, but further measurements should be done in order to confirm or not the presence of this limit.

One characteristic that seems to be common for the majority of the results is that the longer structures present higher increases in their Q-factors after being submitted to annealing temperatures up to 250 ºC, whether their values at lower temperatures are Q ≈ 500 or Q ≈ 2000, despite the need to perform more experiments to validate if this is an acceptable conclusion.

All of these results show that the Q-factors of the tested structures improved, regardless of their length and vibrational mode, when annealed at temperatures up to 250 ºC, thus confirming that annealing is a valid external technique that can be used to improve the Q-factor of any given MEMS resonator. The reason why Q-factors increase when exposed to high temperatures is attributed to the characteristics of the devices at room temperature, where certain conditions such as the presence of water molecules which creates hydration in the surface of the structures, along with surface residues that occur during the process of fabrication, affect the way the devices operate, by lowering their Q-factors. By annealing those devices water dehydrates, and the fabrication residues ashes out, thus improving the mentioned conditions [7].

It can be assumed that water adsorbed on the surface of the structures is one of the sources of surface dissipations, so the way to remove that adsorbed water is to bake the samples [8] in order to improve their Q-factors. The device used for the comparison results was measured for several experiments in this work, during a period of several months. In between those measurements, the *Fres* of the structures were measured three times. By comparing their values, it was demonstrated that the structures do not present major shifts in their intrinsic *Fres*, during a period of around 5 months. These values correspond to measurements in vacuum. The Q-factors were also extracted as it is shown in Graphic 6.

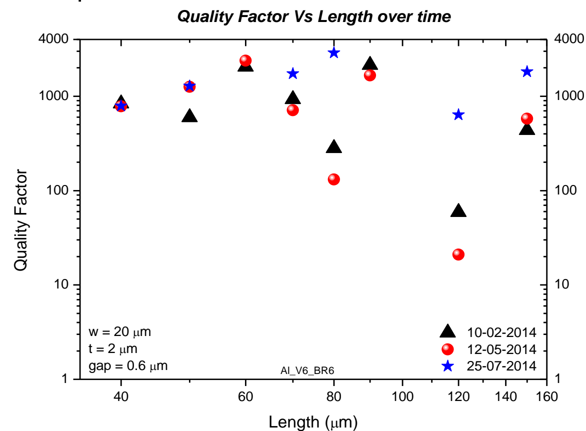


Graphic 6 - Demonstration of the Quality Factor as a function of the Length of the structures for a period of around 5 months

Most of the structures are still measurable after that period of 5 months, and for the majority of them, the Q-factors are relatively comparable.

The main reason why the Q-factors are significantly higher in the last measurement is that it was performed after the annealing process so, besides the increase of the Q-factors when temperature is applied, the structures can maintain those values for quite some time, since the last measurements were performed about a month and a half after the annealing process.

## C. Dissipation in Air

As mentioned before, it is of great importance to estimate the damping characteristics caused by several dissipative media in which MEMS devices can operate. This is an essential analysis since these characteristics will determine the dynamic performance of the system [9] [10].

Some MEMS devices are meant to operate in air, which can lead to some performance issues, where air damping is considered the most problematic energy loss mechanism. Air damping can be defined as the influence of air in a given oscillating device that can reduce or prevent their oscillations. The excess of this effect can determine the performance of the components of

a MEMS device [11]. In order to obtain higher Q-factors and to avoid damping effects, these devices are typically operated at low pressures. Some devices can have very high Q-factors in vacuum. When it is not possible or it is not the purpose of a certain project to operate the structures in vacuum, they must vibrate in certain gases such as air at different variable pressures that can vary from atmospheric to low vacuum [12]. When a vibrating structure interacts with the surrounding media, dissipation occurs which brings the Q-factor down. Factors such as the gap between the gate and the bridge, or the fluid or gas pressure can influence its motion that can range from continuum flow, viscous flow or molecular flow [12] [13], depending on the specificities of the structures. With this in mind, several measurements involving pressure were made to a device contained bridge like structures with 40 μm to 200 μm in length, 10 μm of width and 2 μm of thickness. The gap between the bridges and the gates is 0.6 μm, and the sacrificial layer used in the microfabrication process was Al. This device was exposed to pressure from a range of $10^{-4}$ Torr to atmospheric pressure (760 Torr) at constant AC and DC voltages with the intent of determine the critical pressure ($P_C$), which is the pressure at which the Q-factor of the structure begins to degrade. Regarding the *Fres* of the structures, there were no major shifts in any of the bridges though some of the structures became unmeasurable before the pressure reached atmospheric values. This means that the structures do not present squeeze film damping. In order to understand the differences in flow regimes and to extract the critical pressure ($P_c$) values, the Q-factors of the structures were plotted as a function of the pressure, as it is shown in Graphic 7.

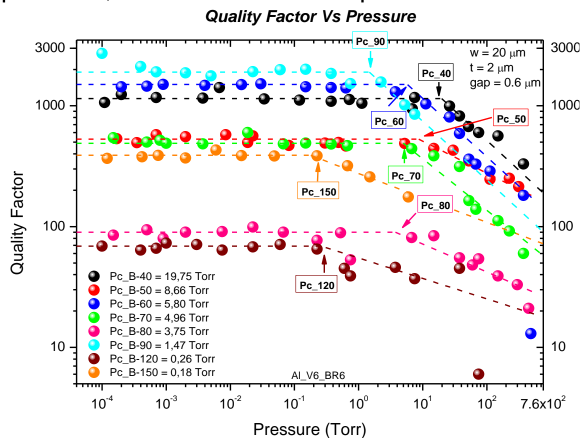


Graphic 7 - Quality Factor as a function of Pressure representation; E=150 GPa; ρ=2330 Kg/m$^3$

For the lower pressure values there are no major Q-factor shifts corresponding to an air flow continuum like regime, where the Q-factors are dominated by intrinsic losses (TED, anchors, etc), since the damping from the medium is considered negligible [12] [13].

Then, it seems that the Q-factor follows different power laws for different size structures. For example, for the 50 μm, 80 μm, 120 μm and 150 μm length bridges the Q-factor appears to follows a power law $Q \propto P^{-1/2}$ corresponding to a viscous flow regime. For other structures like 40 μm, 60 μm, 70 μm and 90 μm in length, the Q-factors appear to depend inversely on the pressure, and the power law $Q \propto P^{-1}$ seems to be followed, corresponding to a free molecular flow regime due to momentum exchange with the individual gas molecules [12] [13]. The reason why the structures that present a free molecular flow regime and not a viscous flow regime is that it was not possible to measure at much higher pressures , otherwise it would be visible a change from the molecular flow to the viscous flow. The results also confirm that Q-factors are pressure dependent.

These results are supported by the theoretical Equations 1 for the viscous flow regime and 2 for the free molecular flow regime [13].

$$Q_{vis} \approx \frac{m_0}{6\pi\mu a^2}\sqrt{\frac{2RT\mu\omega_0}{MP}} \qquad (1)$$

$$Q_{FMF} = \left(\frac{\pi}{2}\right)^{\frac{3}{2}} \rho_r h \frac{\omega}{2\pi}\sqrt{\frac{RT}{M}\frac{1}{P}} \qquad (2)$$

Where $m_0$ is the mass $[Kg]$, μ the viscosity of the fluid $[Kg/m \cdot s]$, a the characteristic linear dimension, R the ideal gas constant, T the temperature $[K]$, $\omega_0$ the angular Resonance Frequency $[rad/s]$, M the molecular mass of the gas medium $[u]$, P the pressure $[Pa]$, $\rho_r$ the mass density $[Kg/m^2]$ and h the thickness $[m]$.

The vibrational modes of these structures were also measured, and the $P_C$ values were extracted for all of the measurable modes, as shown in Graphic 8.

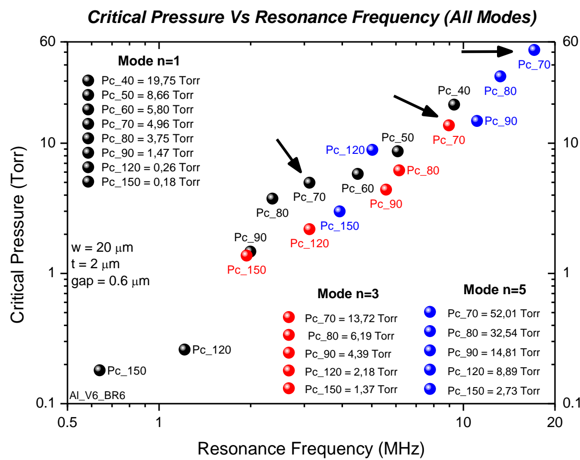

Graphic 8 - Critical Pressures as a function of the Resonance Frequency for all of the vibrational modes

In Graphic 8 it is visible that the shorter structures present higher $P_C$ and the higher vibrational modes of the structures have higher values of $P_c$ when compared to the fundamental mode. It is also clear that the *Fres* is a major factor in these measurements, since any given structures with similar *Fres* will have comparable values of $P_C$, regardless of the vibrational mode. For instance, a very long bridge actuated in a very high vibrational mode, will have similar *Fres* of a fundamental vibrational mode of a shorter structure, therefore their $P_C$ will be close.

## *D. Dissipation in Water*

Despite MEMS devices are well studied in vacuum and air, when testing these structures in dissipative media such as water, some challenges and situations present themselves, like in the case of electrolysis and also electrode charge screening. These are problems that should be avoided due to the fact that they can cause bubbles on the structures, which can lead to defects or other type of damages to the systems [14]. Another common problem that can be encountered when using aqueous media is water-related stiction, which can occur during manufacturing, as well as during the operation of the device when in contact with the fluid used. If these MEMS devices are covered with thin oxide layers due to the lack of surface treatment, that surface will be hydrophilic which is susceptible to large water induced capillary forces that will act in the majority of the contact area [15].

To measure the devices used in this work in a wet dissipative medium, the *Fres* of the structures was measured by submersing them in DI water. The idea is to measure the *Fres* of the structures the same way it was measured in vacuum, but in this case the laser goes through the DI water drop and then is deflected to the photodetector.

To enable this possibility, the wires connecting the device to the chip carrier must be protected with Silicone to avoid the contact with the fluid, as shown in Figures 2 and 3.

The DI water is applied using micropipettes, and its volume can range from 20 μl to 50 μl, depending on the shape of the Silicone well.

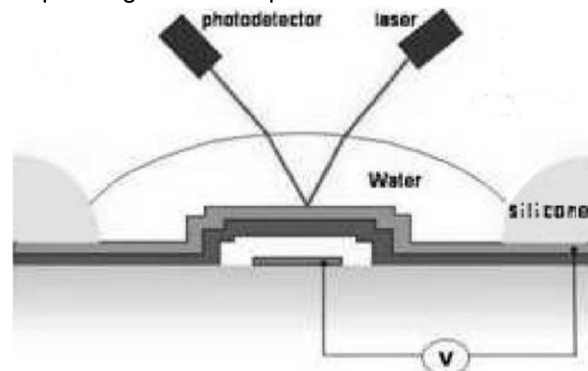

Figure 2 - Schematic illustration of the resonance frequency measurements in DI water [1]

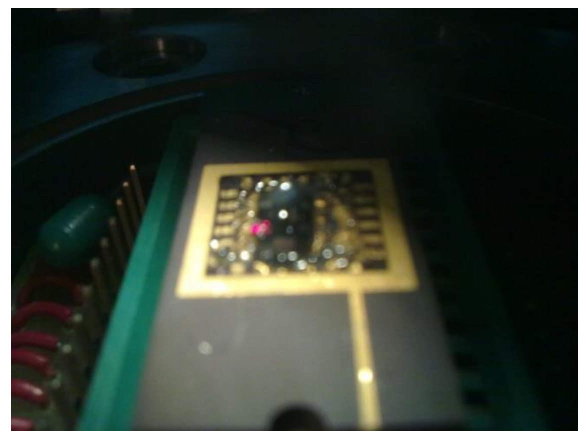
Figure 3 - DI water drop trapped on Silicone well

Graphic 9 demonstrates the shifts of the *Fres* of a 150 μm bridge when exposed to different media.

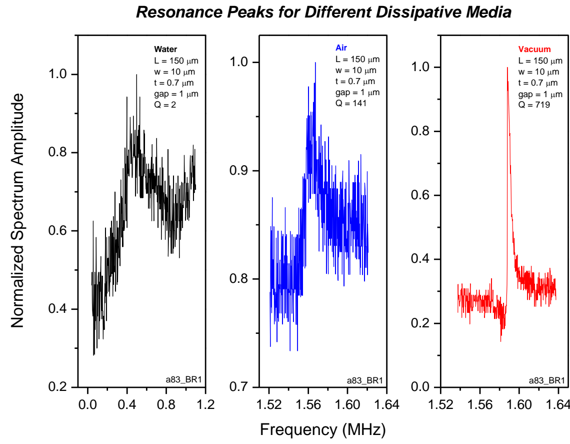

Graphic 9 - Representation of the Frequency peaks of a 150 µm bridge, at different dissipative media

It is visible that for the structure immersed in DI water, there is a shift of the *Fres* to lower values.

That shift increases as the density of the fluid rises, and is relatively small when comparing the results in air and in vacuum [1] [14]. Since the density of water is much higher than the density of air, the shift of the *Fres* will be higher too.

The device used in Chapter III.A was also tested in aqueous media, along with other device from the same run.

These measurements were merely focused on resonance peaks detection in water, so measurements in air were not performed, just in vacuum to validate if some of the structures were functional.

Their Q-factors were extracted as shown in Graphic 10. The applied AC voltages for these structures were 0.6 V ≤ AC ≤ 1 V and the applied DC voltages 0.5 V ≤ DC ≤ 3 V.

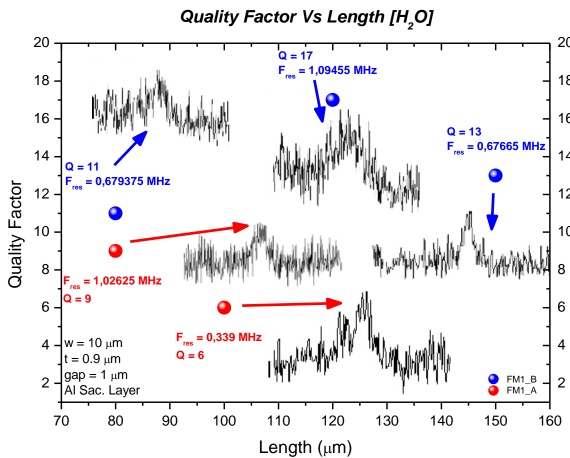

Graphic 10 - Representation of the Quality Factors as a function of the length of the structures, in an aqueous environment, with the correspondent frequency peaks

It is extremely hard to measure a given structure in this type of environment, as it was mentioned before.

For the results above, from the 24 available structures, combining the two devices from Graphic 10, 16 were operational at vacuum. From those, only 5 structures were measurable in this fluidic medium, two from one device and three from the other.

Their Q-factors in vacuum varied from ≈ 50 to ≈ 2000, where the lowest value was Q = 41 and the highest Q = 1981. In DI water, those values decrease significantly, ranging from Q ≈ 2 to Q ≈ 20, where the lowest value was Q = 2 and the highest Q = 17. This last value was the highest Q-factor achieved in this work, for the aqueous environment experiments.

# IV. Conclusions

A voltage bias sweep procedure was performed to verify how different voltages can affect a given structure and to characterize their nonlinearities and mechanical or electrical effects.

Different size structures can be affected by different effects, or even both on the same structure. Most of the measured structures withstand DC voltages up to 30 V without any distortions in their resonance peaks.

Temperature dependence revealed very interesting and conclusive results in the author's opinion, since all of the structures submitted to *annealing* improved their Q-factors regardless of their size, vibrational mode or intrinsic Q-factor, though some ideas and properties were left unconfirmed.

The highest Q-factor achieved in this experiment was Q = 5715 and the structures maintained the higher values achieved after the *annealing* experiment, for almost two months, when the last measurements were made.

A possible threshold limit was also discussed at which the structures with Q-factor above that limit will increase much more, after an abrupt decrease at lower *annealing* temperatures.

The structures are also able to relatively maintain their resonance frequencies in the whole range of applied pressures, which means that they do not present squeeze film damping.

The highest critical point measured was $P_C$ = 52.01 Torr and the highest Q-factor at atmospheric pressure was Q = 490.

Despite the difficulty of extracting frequency peaks in DI water, some Q-factors were extracted. The highest value achieved was 17, for a 120 μm length bridge.

The next step should be the integration of MEMS resonators with microfluidic systems for liquid detection. Simpler resonance frequency detection devices should also be discussed.

To fabricate a successful label-free device, the resonators surface should be functionalized to enable the detection of analyte biomolecules.

## References


[1] T. Adrega, V. Chu and J. P. Conde, "Resonance of electrostatically actuated thin-film amorphous silicon microelectromechanical systems microresonators in aqueous solutions: Effect of solution conductivity and viscosity," *Journal of Applied Physics,* 2007.

[2] E. Timurdogan, B. E. Alaca, I. H. Kavakli and H. Urey, "MEMS biosensor for detection of Hepatitis A and C viruses in serum, Biosensors and Bioelectronics," *Biosensors and Bioelectronics,* pp. 189-194, 2011.

[3] K. M. Hansen and T. Thundat, "Microcantilever biosensors," *Methods,* pp. 57-64, 2005.

[4] D. K. Agrawal, J. Woodhouse, A. A. Seshia, Member and IEEE, "Modeling Nonlinearities in MEMS Oscillators," *IEEE Transactions on Ultrasonics, Ferroelectrics and Frequency Control,* vol. 60, no. 8, 2013.

[5] M. Agarwal, K. K. Park, R. N. Candler, B. Kim, M. A. Hopcroft, S. A. Chandorkar, C. M. Jha, T. W. Kenny and B. Murmann, "Nonlinear Characterization of Electrostatic MEMS Resonators," Standford, California, USA, 2006.

[6] K. Bongsang, Member, IEEE, M. A. Hopcroft, R. N. Candler, Member, IEEE, C. M. Jha, Student Member, ASME, M. Agarwal, Member, IEEE, R. Melamud, S. A. Chandorkar, G. Yama and T. W. Kenny, "Temperature Dependence of Quality Factor in MEMS Resonators," *Journal of Microelectromechanical Systems,* vol. 17, no. 3, 2008.

[7] M. J. Ahamed, D. Senkal and A. M. Shkel, "Effect of Annealing on Mechanical Quality Factor of Fused Quartz Hemispherical Resonator," Irvine, CA, USA, 2014.

[8] V. P. Mitrofanov and K. V. Tokmakov, "Effect of heating on dissipation of mechanical energy in fused silica fibers," *Physics Letters A,* no. 308, pp. 212-218, 2003.

[9] M. Imboden, O. A. Williams and P. Mohanty, "Observation of Nonlinear Dissipation in Piezoresistive Diamond Nanomechanical Resonators by Heterodyne Down-Mixing," *Nano Letters,* vol. 13, pp. 4014-4019, 2013.

[10] H. Hosaka, K. Itao and S. Kuroda, "Damping characteristics of beam-shaped micro-oscillators," *Sensors and Actuators A,* vol. 49, pp. 87-95, 1995.

[11] S. Gorelick, J. R. Dekker, M. Leivo and U. Kantojärvi, "Air Damping of Oscillating MEMS Structures: Modeling and Comparison with Experiment," in *COMSOL Conference*, Rotterdam, 2012.

[12] A. K. Pandey, R. Pratap and F. S. Chau, "Effect of Pressure on Fluid Damping in MEMS Torsional Resonators with Flow Ranging from Continuum to Molecular Regime," *Experimental Mechanics,* vol. 48, pp. 91-106, 2008.

[13] A. Gualdino, V. Chu and J. P. Conde, "Pressure effects on the dynamic properties of hydrogenated amorphous silicon disk resonators," *Journal of Micromechanics and Microengineering,* vol. 22, 2012.

[14] T. Adrega, V. Chu and J. P. Conde, "Electrostatically actuated resonance of amorphous silicon microresonators in water," *Applied Physics Letters,* vol. 89, 2006.

[15] M. Scherge, X. Li and J. A. Schaefer, "The effect of water on friction of MEMS," *Tribology Letters,* vol. 6, pp. 215-220, 1998.